PNAS BRIEF REPORT | APPLIED PHYSICAL SCIENCES
BIOPHYSICS AND COMPUTATIONAL BIOLOGY OPEN ACCESS

The ergodicity question when imaging DNA conformation using liquid cell electron microscopy

Jia-Ye Li[a,1], Fan Liu[a,b,1], Jing Xu[a,b], Ye-Jin Kim[c,d], Oh-Hoon Kwon[c,d], Bin Xia[a,b], Huan Wang[a,2], and Steve Granick[c,d,e,2]

Edited by John Rogers, Northwestern University, Evanston, IL; received August 28, 2023; accepted November 28, 2023

Assessing the ergodicity of graphene liquid cell electron microscope measurements, we report that loop states of circular DNA interconvert reversibly and that loop numbers follow the Boltzmann distribution expected for this molecule in bulk solution, provided that the electron dose is low (80-keV electron energy and electron dose rate 1–20 e^- $Å^{-2}$ s^{-1}). This imaging technique appears to act as a "slow motion" camera that reveals equilibrated distributions by imaging the time average of a few molecules without the need to image a spatial ensemble.

TEM | graphene liquid cell | ergodicity

Imaging the rich conformational substates of biomacromolecules requires that one slow their interconversion rate, as in bulk aqueous solution, it is prohibitively rapid. Here, we assess the potential of graphene liquid cell (GLC) transmission electron microscopy (TEM) to accomplish this goal. This technique originated in the study of nanoparticles (1, 2) and ubiquitously showed diffusion slowed by a factor of 10^8, reflecting enhanced interfacial viscosity (3–5) or more likely transient adsorption (6). Diffusion of DNA oligomers is slowed by roughly the same factor (7). Although recognizing the possible perturbative influence of electron energy and electron dose (8), we conjectured that flexible molecules explore conformations similar to those in free solution when they are near the adsorption–desorption transition. A test of ergodicity—whether ensemble-average coincides with time average—should concern a molecule sufficiently simple to compare to theory with sufficient dynamic range. To provide this test, we selected circular DNA (9).

We work with a closed-loop (circular) double-stranded DNA (dsDNA) of 336 bp (10), dissolved in dilute aqueous solution, confined between atomically thin graphene sheets <100 nm in height, which is sufficiently thin to resolve individual molecules without prohibitive background electron scattering (1). Each displays time-dependent numbers of loops, and their relative abundance reflects the relative energetics. The first imaging condition (A) was H_2O, 44 molecules in 11 GLCs, electron dose rate 5–20 e^- $Å^{-2}$ s^{-1}, each movie containing several hundred frames with 21,000 images total. The second (B) was D_2O to prolong the imaging time by retarding bubble formation (11) (16 molecules in five GLCs). The third (C) was electron dose rate 1–5 e^- $Å^{-2}$ s^{-1} in H_2O (14 molecules in two GLCs). The fourth (D) was electron dose rate 1–5 e^- $Å^{-2}$ s^{-1} in D_2O (21 molecules in five GLCs). Ten thousand images were obtained for each condition in (B), (C), and (D), 53,496 images in total including (A). The GLC setup is shown schematically in Fig. 1*A*. The persistence length of dsDNA is 50 nm (150 bp), so this sample 336 bp long is flexible with curvature reflected in the number of loops, N. Theory predicts that bending energy is proportional to N^2 (12).

Results

Distributions of Loop Number *N* Suggest Ergodicity. An ergodic molecule should exhibit molecular states whose energy distribution obeys Boltzmann distribution. We observe up to $N = 4$ loops and quantify them using an image analysis algorithm (13). Fig. 1*A* shows examples. State $N = 1$ is most abundant; loop incidence decreases with N and interconversion is reversible. Loop number N are predominantly in sequence as illustrated in Fig. 1*B* and Movie S1 but occasional molecules skip a loop state, for example, transforming from $N = 3$ to $N = 1$. These features, expected in equilibrium, suggest that our dataset is sufficiently large to include states of low probability.

The distributions of N are insensitive to imaging condition; the difference across imaging conditions is similar to the uncertainty for any single imaging condition. Fig. 1*C*, relative probability plotted against N^2, shows consistency with the Boltzmann relation anticipated for an equilibrated distribution of independent molecules (37,247, 12,742, 3,191, and 316 images for $N = 1$, 2, 3, and 4, respectively). As shown in Fig. 1*C*, differences between different imaging conditions are second order. Grouping together the data from four

Author affiliations: [a]Beijing National Laboratory for Molecular Sciences, College of Chemistry and Molecular Engineering, National Biomedical Imaging Center, Key Laboratory of Polymer Chemistry & Physics of Ministry of Education, Peking University, Beijing 100871, China; [b]Beijing NMR Center, School of Life Science, Peking University, Beijing 100871, China; [c]Department of Chemistry, Ulsan National Institute of Science and Technology, Ulsan 44919, South Korea; [d]Center for Soft and Living Matter, Institute for Basic Science, Ulsan 44919, South Korea; and [e]Department of Polymer Science and Engineering, University of Massachusetts, Amherst, MA 01003

Author contributions: H.W. and S.G. designed research; J.-Y.L. and H.W. performed research; F.L., J.X., Y.-J.K., O.-H.K., and B.X. contributed new reagents/analytic tools; H.W. and S.G. analyzed data; and H.W. and S.G. wrote the paper.

The authors declare no competing interest.

[1]J.-Y.L. and F.L. contributed equally to this work.

[2]To whom correspondence may be addressed. Email: wanghuan_ccme@pku.edu.cn or sgranick@umass.edu.

This article contains supporting information online at https://www.pnas.org/lookup/suppl/doi:10.1073/pnas.2314797121/-/DCSupplemental.

Published January 9, 2024.

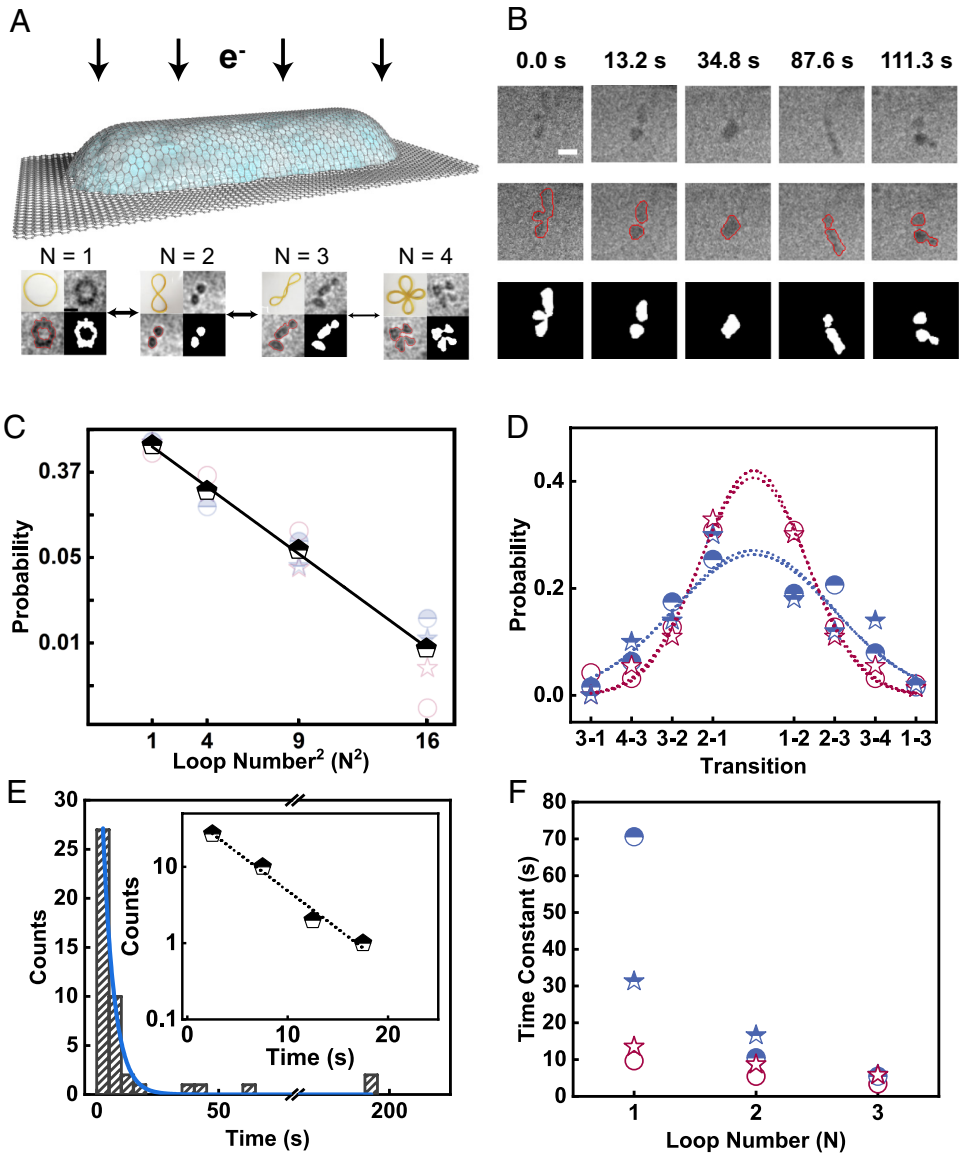

Fig. 1. Cyclic DNA molecules imaged in GLCs using TEM. (*A*) Schematic illustration of the GLC in which we image interconversion between loop numbers N = 1, 2, 3, and 4. The four images for each N show schematic sketch of this N (*Top Left*), its electron micrograph (*Top Right*), image processed using the software algorithm UNet++ with red circles identifying the loop state (*Bottom Left*), and binarized image for improved visual contrast (*Bottom Right*). (Scale bar, 10 nm.) Double-headed arrows indicate reversible interconversion between neighboring states, thicker according to relative frequency. (*B*) Time-resolved images for the pathway N = 3–2–1–2–3. Exposure time is 0.3 s, Scale bar is 10 nm, with images (*top* row), analyzed using the software UNet++, with red circles identifying the loop state (*middle* row), and binarized images for better visual contrast (*third* row). (*C*) Relative probabilities of N plotted against N^2. Black pentagons represent all data points. Data obtained under four imaging conditions: open stars (A), open circles (B), half-filled stars (C), and half-filled circles (D). (*D*) Relative probabilities of interconversion between N specified in abscissa. Symbols are the same as in panel *C*. (*E*) For imaging condition B and N = 1, illustrative histogram of duration time used to obtain τ with line showing exponential fit. *Inset*: Same data on semilogarithmic scales. (*F*) Time constants τ plotted against N with the same symbols as in panel *D*.

imaging conditions, there is no systematic dependence on the imaging condition and from the Boltzmann equation, the energy difference between given loop numbers is 1 to 2 k_BT. The slope of linear regression fit to the average dataset is 0.3 with correlation coefficient R^2 = 0.998. For each state-to-state transition, the product of slope in Fig. 1*C* and the difference of squared loop number for each of these states is the activation energy, giving ΔE_{12}, ΔE_{23}, ΔE_{34} = 0.9 ± 0.2, 1.6 ± 0.3, and 2.2 ± 0.4 k_BT, respectively (uncertainty is the SD).

Kinetic Pathways Depend on Electron Dose. Within the experimental time window, the interconversion between states should be reversible for an ergodic system. Reversible transformations, tallied in Fig. 1*D* as relative probabilities, are symmetric within experimental uncertainty for imaging conditions (A) and (B) but slightly asymmetric for imaging conditions (C) and (D), for which we observe a higher frequency of N = 2 to N = 1 than the reverse process. The N = 1 state may be statistically stabilized by having more points of surface contact when the electron dose is low. Interestingly, the transition probabilities are similar in H_2O and D_2O despite the adsorption isotope effect (14). This suggests that electron dose is the stronger influence. From histograms of duration time between conformational transitions, we inferred time constants τ illustrated in Fig. 1*E*. They decrease with increasing N as expected since looped states are less stable (Fig. 1*F*). Although absolute values of τ depend on the imaging condition, their ratios do not. Estimating free energy differences from this ratio, we obtain estimates for ΔE_{12}, ΔE_{23}, and ΔE_{34} =

1.6, 1.5, and 2.5 k_BT, respectively, consistent with the estimates obtained from Fig. 1*C*.

Discussion

Our data are ergodic within experimental uncertainty. These data support the view that the GLC–TEM imaging technique acts as a "slow motion" camera, revealing intermediate states too fleeting to be captured in bulk solution, yet characteristic of bulk solution owing to the tradeoff between adsorption to graphene, which tends to stabilize low-energy conformations, and electron dose which tends to facilitate interconversion to higher-energy states. Speculatively, this technique has opportunity, also for other biomacromolecules, to investigate conformational rearrangements when macromolecules encounter one another.

Materials and Methods

We synthesized 336-bp minicircles by procedures described previously (15) with a minicircle plasmid pTUBB3-MC (gift from Juan Belmonte, Addgene plasmid #87112; http://n2t.net/addgene:87112; RRID: Addgene_87112) using the ClonExpress II One Step Cloning Kit (Vazyme). We purchased Quantifoil@R 1.2/1.3 gold grids with a mesh size 300 from SPI Supplies. The 2-layer and 3- to 5-layer graphene grown by CVD on copper was bought from ACS Material. We formed GLCs from graphene scrolls or creases (6) and used common electron microscope: a JEOL-2100 TEM equipped with a direct electron-detection camera (K2 summit, Gatan) or a Gatan Oneview IS camera. Images were processed and analyzed (13) with details in *SI Appendix*.

Data, Materials, and Software Availability. All study data are included in the article and/or supporting information.

ACKNOWLEDGMENTS. We thank the Center for Spectroscopic Analysis, and the Electron Microscopy Facility in the Analytical Instrumentation Center of Peking University.

1. J. M. Yuk *et al.*, High-resolution EM of colloidal nanocrystal growth using graphene liquid cells. *Science* **336**, 61–64 (2012).
2. J. Park *et al.*, Graphene liquid cell electron microscopy: Progress, applications, and perspectives. *ACS Nano* **15**, 288–308 (2021).
3. A. Verch, M. Pfaff, N. de Jonge, Exceptionally slow movement of gold nanoparticles at a solid/liquid interface investigated by scanning transmission electron microscopy. *Langmuir* **31**, 6956–6964 (2015).
4. S. Kang *et al.*, Real-space imaging of nanoparticle transport and interaction dynamics by graphene liquid cell TEM. *Sci. Adv.* **7**, eabi5419 (2021).
5. J. Lu, Z. Aabdin, N. D. Loh, D. Bhattacharya, U. Mirsaidov, Nanoparticle dynamics in a nanodroplet. *Nano Lett.* **14**, 2111–2115 (2014).
6. H. Wang, Z. Xu, S. Mao, S. Granick, Experimental guidelines to image transient single-molecule events using graphene liquid cell electron microscopy. *ACS Nano* **11**, 18526 (2022).
7. H. Wang, B. Li, Y.-J. Kim, O.-H. Kwon, S. Granick, Intermediate states of molecular self-assembly from liquid-cell electron microscopy. *Proc. Natl. Acad. Sci. U.S.A.* **117**, 1283–1292 (2020).
8. J. Kim, M. R. Jones, Z. Ou, Q. Chen, In situ electron microscopy imaging and quantitative structural modulation of nanoparticle superlattices. *ACS Nano* **10**, 9801–9808 (2016).
9. J. S. Mitchell, S. A. Harris, Thermodynamics of writhe in DNA minicircles from molecular dynamics simulations. *Phys. Rev. Lett.* **110**, 148105 (2013).
10. M. A. Kay, C.-Y. He, Z.-Y. Chen, A robust system for production of minicircle DNA vectors. *Nat. Biotechnol.* **28**, 1287–1289 (2010).
11. H. Wang, K. H. Nagamanasa, Y.-J. Kim, O.-H. Kwon, S. Granick, Longer-lasting electron-based microscopy of single molecules in aqueous medium. *ACS Nano* **12**, 8572–8578 (2018).
12. J. F. Marko, "DNA mechanics" in *Nuclear Architecture and Dynamics*, C. Lavelle, J.-M. Victor, Eds. (Academic Press, 2018), pp. 3–40.
13. B. Cheng, E. Ye, H. Sun, H. Wang, Deep learning-assisted analysis of single molecule dynamics from liquid-phase electron microscopy. *Chem. Commun.* **59**, 1701–1704 (2023).
14. P. Frantz, D. C. Leonhardt, S. Granick, Enthalpic effects in competitive polymer adsorption: Adsorption isotope effect and chain end effect. *Macromolecules* **24**, 1868–1875 (2002).
15. M. A. Kay, C.-Y. He, Z.-Y. Chen, A robust system for production of minicircle DNA vectors. *Nat. Biotechnol.* **28**, 1287–1289 (2010).